JOURNAL OF ENVIRONMENTAL SCIENCES 84 (2019) 69–79

Available online at www.sciencedirect.com

ScienceDirect

www.elsevier.com/locate/jes

JES JOURNAL OF ENVIRONMENTAL SCIENCES

www.jesc.ac.cn

Photocatalytic defluorination of perfluorooctanoic acid by surface defective BiOCl: Fast microwave solvothermal synthesis and photocatalytic mechanisms

Yuanyuan Sun[1], *Guiying Li*[1], *Wanjun Wang*[1,*], *Wenquan Gu*[1], *Po Keung Wong*[2], *Taicheng An*[1]

1. *Guangzhou Key Laboratory Environmental Catalysis and Pollution Control, Guangdong Key Laboratory of Environmental Catalysis and Health Risk Control, School of Environmental Science and Engineering, Institute of Environmental Health and Pollution Control, Guangdong University of Technology, Guangzhou 510006, China*

2. *School of Life Sciences, The Chinese University of Hong Kong, Shatin, New Territories, Hong Kong, China*

ARTICLE INFO

Article history:
Received 14 February 2019
Revised 15 April 2019
Accepted 17 April 2019
Available online 25 April 2019

Keywords:
Photocatalysis
Perfluorooctanoic acid
Oxygen vacancy
Microwave method
BiOCl

ABSTRACT

There is an urgent need for developing cost-effective methods for the treatment of perfluorooctanoic acid (PFOA) due to its global emergence and potential risks. In this study, taking surface-defective BiOCl as an example, a strategy of surface oxygen vacancy modulation was used to promote the photocatalytic defluorination efficiency of PFOA under simulated sunlight irradiation. The defective BiOCl was fabricated by a fast microwave solvothermal method, which was found to induce more surface oxygen vacancies than conventional solvothermal and precipitation methods. As a result, the as-prepared BiOCl showed significantly enhanced defluorination efficiency, which was 2.7 and 33.8 times higher than that of BiOCl fabricated by conventional solvothermal and precipitation methods, respectively. Mechanistic studies indicated that the defluorination of PFOA follows a direct hole (h^+) oxidation pathway with the aid of •OH, while the oxygen vacancies not only promote charge separation but also facilitate the intimate contact between the photocatalyst surface and PFOA by coordinating with its terminal carboxylate group in a bidentate or bridging mode. This work will provide a general strategy of oxygen vacancy modulation by microwave-assisted methods for efficient photocatalytic defluorination of PFOA in the environment using sunlight as the energy source.

Introduction

Perfluorooctanoic acid (PFOA) belongs to the family of fully fluorinated hydrocarbons, and has been regarded as an emerging persistent organic pollutant. It has attracted increasing worldwide concern because of its global emergence and high bioaccumulation ability (Lindstrom et al., 2011). For example, PFOA has recently been found in humans, animals, environmental water, and even in some living beings in remote polar regions (Liu et al., 2018; Skutlarek et al., 2006;

* *Corresponding author. E-mail:* wanjun@gdut.edu.cn (Wanjun Wang).

https://doi.org/10.1016/j.jes.2019.04.012

Sungur, 2018). Recent toxicological studies have already shown that PFOA could lead to irreversible growth and reproductive toxicity and kidney damage, as well as potential cancer risks (Song et al., 2018; Stanifer et al., 2018). Therefore, cost-effective technologies for efficient decomposition of PFOA are urgently needed.

However, because of the strong carbon–fluorine bonds, PFOA has extremely high thermal and chemical stability. It resists most conventional treatment processes such as thermolysis, photolysis, and biological degradation (Sinclair and Kannan, 2006). Previous studies have shown that advanced oxidation technologies (AOPs) such as ultraviolet light (UV)-Fenton (Tang et al., 2012), high-frequency ultrasonication (Moriwaki et al., 2005), electrochemical methods (Lin et al., 2018), persulfate oxidation (Lee et al., 2013) and photocatalysis (Sahu et al., 2018) can be employed to decompose such halogenated organic pollutants. Among these, photocatalysis has attracted ever-increasing attention because inexhaustible solar light is expected to be utilized to drive the reaction process, which has low energy consumption and fulfills the requirements of sustainable development. However, the dominant reactive species commonly identified in the photocatalytic process, hydroxyl radical (•OH), has been hypothesized to be less effective for the decomposition of PFOA (Zhao et al., 2012). For instance, the defluorination efficiency of PFOA was reported to be only ~5.3% using TiO_2 as photocatalyst combined with ultrasonication in 8 hr of treatment time (Panchangam et al., 2009a). Fortunately, it has been recently revealed that photo-generated holes seem to be more effective for the defluorination of PFOA (Zhong et al., 2019). For example, Panchangam et al. (2009b) found that the PFOA defluorination efficiency could be greatly improved via a direct hole (h^+)-oxidation pathway in the TiO_2 system. Moreover, several other metal oxides such as Ga_2O_3, In_2O_3 and InOOH have also been reported to possess degradation ability for PFOA via direct h^+ oxidation (Li et al., 2012; Shao et al., 2013; Xu et al., 2017). It was suggested that PFOA could be tightly connected to the photocatalyst surface via a certain coordination mode through the carboxylate group, which would favor direct h^+ attack. On the other hand, surface defect modulation has become an emerging strategy for improving the photocatalytic activity of semiconductors (Pan et al., 2013). For example, the creation of oxygen vacancies on BiOCl, a layered bismuth oxyhalide photocatalyst, has been well-established as a facile way to promote its photocatalytic activity by decreasing the band gap and inhibiting the recombination of photogenerated electron (e^-)–h^+ pairs (Cui et al., 2018; Li et al., 2014; Zhao et al., 2013). If the carboxylate group of PFOA could be precisely anchored onto surface oxygen defects, it would create an avenue for its subsequent direct oxidation by photo-generated h^+. However, such role of oxygen vacancies in the sunlight-driven photocatalytic defluorination of PFOA has not been well investigated and illustrated in previous reports.

Over past decades, microwave-assisted methods have become a cost-effective and facile pathway to synthesize various nanomaterials such as ZnO (Kashinath et al., 2015), TiO_2 (Tian et al., 2019) and Fe_2O_3 (Sun et al., 2016). The uniform and rapid microwave heating is expected to produce nanoparticles with narrower size distributions as well as higher purities than those produced by ordinary heating methods (Chen et al., 2009; Hassan et al., 2018; Kim et al., 2014). Besides, microwave-assisted heating is also believed to shorten the fabrication time and enhance the degree of crystallinity, which also results in products with large surface areas, pore volumes and pore widths. Unfortunately, the function of microwave heating of creating oxygen vacancies on metal oxides to promote the photocatalytic defluorination of PFOA has not been studied previously.

In this work, taking BiOCl as the example due to its oxygen vacancy-dependent photocatalytic properties and facile oxygen vacancy generating capacity, we endeavored to investigate the function of surface oxygen vacancies in the photocatalytic defluorination of PFOA under simulated sunlight irradiation. The formation of surface-defective BiOCl was achieved by a microwave solvothermal method. For comparison, the synthesis of BiOCl by conventional solvothermal and precipitation methods was also carried out to evaluate their activity for the defluorination of PFOA. This work will provide useful information on developing new strategies to design and fabricate efficient photocatalysts for decomposition of persistent perfluorocarboxylic acids under mild conditions, thus eliminating their potential hazard to environmental water bodies.

1. Materials and methods

1.1. Synthesis of defective BiOCl and characterization

BiOCl with surface oxygen vacancies was fabricated by a microwave solvothermal method. The synthesis procedure was modified from a conventional solvothermal method (Cui et al., 2018). The major modification was that microwave heating was applied. For comparison, BiOCl was also synthesized by the conventional solvothermal method, as well as by a precipitation method according to the literature (Song et al., 2017). The samples synthesized by the precipitation method, conventional solvothermal method and microwave solvothermal method were denoted as a-BiOCl, b-BiOCl and c-BiOCl, respectively. The detailed synthesis procedures and characterization methods can be found in Appendix A. Supplementary data.

1.2. Photocatalytic defluorination of PFOA

A homemade water-jacketed cylindrical quartz reactor was used for the experiments on photocatalytic decomposition of PFOA under simulated solar irradiation. In a typical experiment, 100 mg of the as-prepared BiOCl photocatalysts was added to 100 mL PFOA solution (50 μmol/L) under stirring. The obtained suspension was then stirred in the dark without light irradiation for 30 min to achieve PFOA adsorption equilibrium. Subsequently, the suspension was irradiated by a 300 W xenon lamp (PLS-SXE300, PerfectLight, China) with an AM 1.5 filter to simulate sunlight irradiation. The light intensity was 105 mW/cm^2, and the reaction temperature was maintained at 30 ± 2°C. At given time intervals, aliquots of the sample suspension were taken and centrifuged at

16,000 r/min for 5 min. After that, the resulting liquid was further filtered through a 0.22 μm membrane to remove sample particles before analysis. The first 2 mL of the resulting filtrate was discarded to avoid the possible influence of PFOA adsorption on the membrane filters. For scavenging studies, isopropanol, sodium oxalate and 4-hydroxy-2,2,6,6-tetramethylpiperidin-1-oxyl (TEMPOL) with concentrations of 5 mmol/L were used as •OH, h^+ and $•O_2^-$ scavengers, respectively.

1.3. Analysis

The PFOA concentration was measured by using high performance liquid chromatography – triple quadrupole tandem mass spectrometry (MS) (1260-6470, Agilent, USA). A binary mixture solution was used as the mobile phase, composed of 5% solvent A (0.1% acetic acid in water) and 95% solvent B (100% methanol). The flow rate was set at 0.4 mL/min. The aliquot injection volume was 5 μL, and the column was equilibrated for 3 min with total running time of 10 min. The multiple reaction monitoring (MRM) mode was applied for the tandem MS analysis. The collision energy and cone voltage were set at 5 and 30 V, respectively. Ion chromatography (761 compact IC, Metrohm, Switzerland) was used to determine the released F^- concentrations during the PFOA decomposition processes. A Metrosep A Supp 5 column (150 mm × 4.0 mm) with Metro A Guard column (5 mm × 4.0 mm) was used for analysis. The mobile phase was a mixed solution containing Na_2CO_3 (3.2 mmol/L) and $NaHCO_3$ (1 mmol/L) with flow rate set at 1.0 mL/min. The defluorination efficiency (DF) during the photocatalytic treatment was then estimated by the equation:

$$\mathrm{DF} = \frac{C_{F^-}}{C_0 \times 15} \times 100\% \tag{1}$$

where, C_F^- represents the released F^- concentration during the photocatalytic treatment process, and C_0 is the initial PFOA concentration before treatment, and "15" denotes the number of F atom in PFOA molecule.

2. Results and discussion

2.1. Materials characterization

Fig. 1a exhibits the obtained diffraction patterns of the microwave solvothermal synthesized BiOCl (c-BiOCl) together with those of the BiOCl synthesized by the conventional solvothermal method (b-BiOCl) and precipitation method (a-BiOCl) for comparison. It was clear that all three XRD

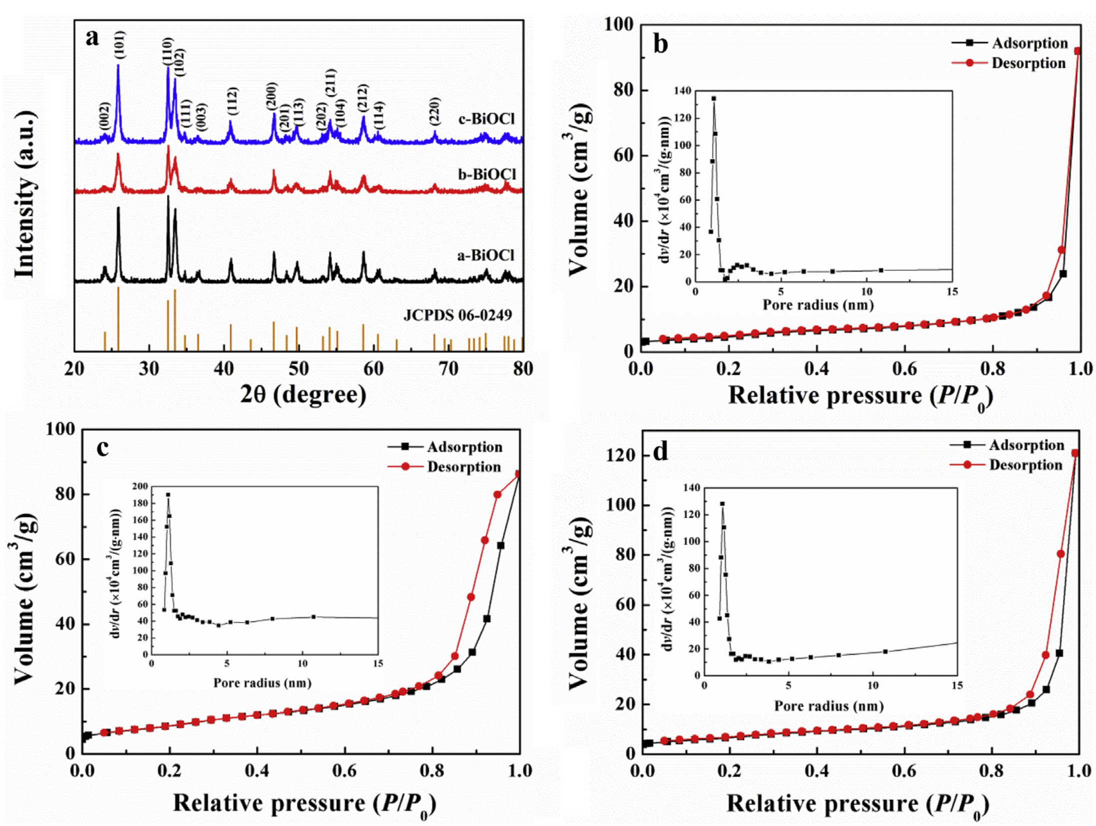

Fig. 1 – (a) X-ray diffraction (XRD) patterns of the as-prepared BiOCl samples synthesized by precipitation method (a-BiOCl), conventional solvothermal method (b-BiOCl), and microwave solvothermal method (c-BiOCl); N_2 adsorption–desorption isotherms with an inset pore-size distribution plot for (b) a-BiOCl, (c) b-BiOCl and (d) c-BiOCl. d*v*/d*r*: the rate of change of pore volume with pore size, where *v* represents the pore volume, and *r* represents the pore diameter.

diffraction patterns can be well-indexed to the BiOCl structure with tetragonal phase and JCPDS No. of 06-0249. The lattice parameters were determined as $a = 0.3891$ nm and $c = 0.7369$ nm. No other impurities were found, indicating that all three methods can result in high purity BiOCl. However, the reaction time of the microwave solvothermal method was much shorter than that of the conventional solvothermal method, because microwave irradiation can lead to localized intense heating of the solution, leading to a drastic increase in the reaction kinetics (Chen et al., 2009). Fig. 1b–d represent the nitrogen adsorption–desorption isotherms of the three as-prepared BiOCl samples with pore size distribution curves. According to the International Union of Pure and Applied Chemistry (IUPAC) classification, all three samples showed isotherms which should be classified as type IV, with the hysteresis loop similar to type H3. This suggests the samples possess a mesoporous structure, which may originate from interparticle stacking (Wang et al., 2008b). The average pore size is about 1–2.5 nm with a narrow distribution (inset of Fig. 1b–d). Compared with a-BiOCl, b-BiOCl and c-BiOCl exhibited a much larger hysteresis loop, suggesting that b-BiOCl and c-BiOCl have larger pore volumes and specific surface areas. The obtained Brunauer–Emmett–Teller (BET) surface area was 18.3, 33.1 and 25.1 m^2/g for a-BiOCl, b-BiOCl and c-BiOCl, respectively. These results indicate that the samples synthesized by the solvothermal methods have larger surface areas than that synthesized by the precipitation method.

The morphologies of the samples were studied by scanning electron microscopy (SEM, SU8220, Hitach, Japan) and transmission electron microscopy (TEM, Talos F200s, FEI, USA) observation. As shown in Fig. 2, the sample synthesized by the precipitation method exhibits large irregular particles (Fig. 2a), while the sample fabricated by the conventional solvothermal method shows a nanoparticle morphology with sizes in the range of 20–50 nm (Fig. 2b), indicating that the solvothermal method tends to produce nanomaterials, as reported by previous studies (Zhang et al., 2017). Interestingly, the BiOCl fabricated by the microwave solvothermal method shows a nanosheet-like morphology with thickness of 20–50 nm and side length of about 100 nm, with the sheets stacked together to form a hierarchical structure (Fig. 2c). The respective energy dispersive spectroscopy (EDS) spectrum of c-BiOCl is shown in Fig. 2d, which further confirms the presence of Bi, Cl and O without other impurities. The signal of C derives from the conducting substrates. It is also found that the atomic molar ratio of bismuth: chlorine: oxygen in c-BiOCl is close to 1:1:0.74, suggesting that considerable numbers of oxygen vacancies are formed on the photocatalyst surface. The typical TEM images in Fig. 3a further confirm the nanosheet morphology. In addition, the HRTEM images reveal that the nanosheet sample possesses a high degree of crystallinity with clear lattice fringes. As shown, the lattice spacing of ~ 0.73 nm, which is indexed to (001) facets (the top view, Fig. 3b), and a lattice spacing of ~0.263 nm, which is indexed to (110) facets (the side view, Fig. 3c), are clearly observed. Therefore, the exposed bottom and top surfaces of the c-BiOCl with nanosheet morphology

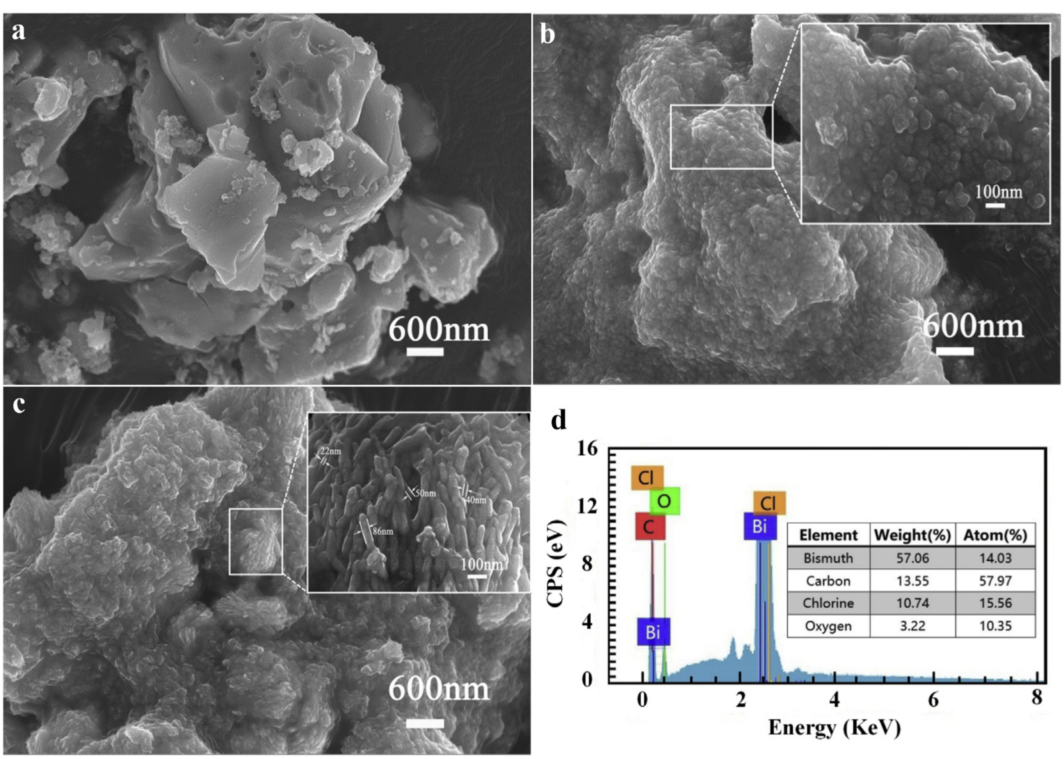

Fig. 2 – Typical scanning electron microscopy (SEM) images of (a) a-BiOCl, (b) b-BiOCl, (c) c-BiOCl and (d) corresponding energy dispersive spectroscopy (EDS) spectrum of c-BiOCl.

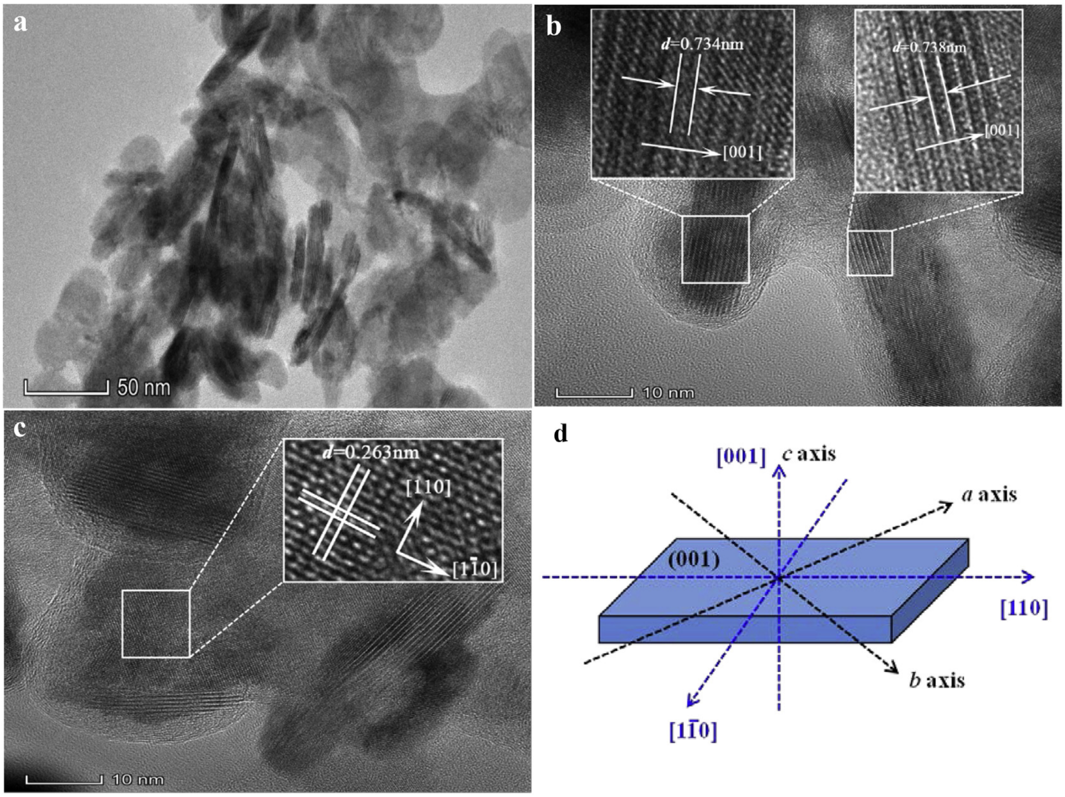

Fig. 3 – (a) Typical transmission electron microscopy (TEM) images, (b) top view of high resolution transmission electron microscopy (HRTEM) images and (c) side view of HRTEM images of c-BiOCl nanosheets; (d) simulated structure of single c-BiOCl nanosheet.

can be identified as (001) facets (Fig. 3d). This exposed facet is beneficial for generating more oxygen vacancies, since the oxygen atom density on (001) facets is higher than on other facets, according to a previous study (Ye et al., 2011).

The light absorption properties of the three samples were determined by using ultraviolet–visible diffuse reflectance spectra (UV–Vis DRS). For a-BiOCl, the light absorption cutoff wavelength is about 355 nm, while a noticeable red shift towards the visible light region is observed in the cases of b-BiOCl and c-BiOCl (Appendix A Fig. S1a). The following equation can be used to evaluate the band gap energy (E_g) of a semiconductor (Wang et al., 2013):

$$\alpha h\nu = A\left(h\nu - E_g\right)^n \tag{2}$$

where, α is the absorption coefficient, $h\nu$ is the photon energy, A is a constant, and $n = 2$ for BiOCl as an indirect transition semiconductor (Hu et al., 2014). Therefore, E_g can be measured by plotting a graph of $(\alpha h\nu)^{1/2}$ vs. $h\nu$. As shown in Appendix A Fig. S1b, E_g is determined to be about 3.38 eV for a-BiOCl, 3.31 eV for b-BiOCl and c-BiOCl, respectively. The reason for the observed band-gap narrowing of BiOCl may be the result of the overlapping of defective electronic states (Li et al., 2014). This suggests that a considerable concentration of oxygen vacancies is produced on b-BiOCl and c-BiOCl. In addition, compared with b-BiOCl, the c-BiOCl sample showed a more intense absorption tail in the visible light region of 400–800 nm, which can be explained by the interband states positioned within the band gap caused by surface oxygen vacancies, as reported by previous studies (Cushing et al., 2017; Dong et al., 2015), suggesting that the microwave solvothermal method can lead to more surface oxygen vacancies than the conventional solvothermal method. Moreover, the corresponding color change of the three samples is demonstrated, as shown in the inset of Appendix A Fig. S1a. The a-BiOCl sample exhibited a white color as expected, since no oxygen vacancies were produced. In contrast, the colors of b-BiOCl and c-BiOCl gradually changed from light-yellow to yellowish-gray, suggesting that the numbers of oxygen vacancies increased, which leads to the change in color. This provides the intuitive observation that the sample prepared by the microwave solvothermal method could have more oxygen vacancies.

Electron paramagnetic resonance (EPR) spectroscopy (EMXPlus, Bruker, USA) was applied to study the surface defects to further confirm the existence of oxygen vacancies. As shown in Fig. 4a, both b-BiOCl and c-BiOCl samples show distinct signals with dimensionless magnetic moment (g-value) of 2.002. This signal matches well with previous studies, and results from electrons that are trapped in formed oxygen vacancies (Kong et al., 2011). In addition, the higher signal intensity of c-BiOCl illustrates that the BiOCl obtained by the microwave solvothermal method has significantly higher concentrations of oxygen vacancies than that prepared

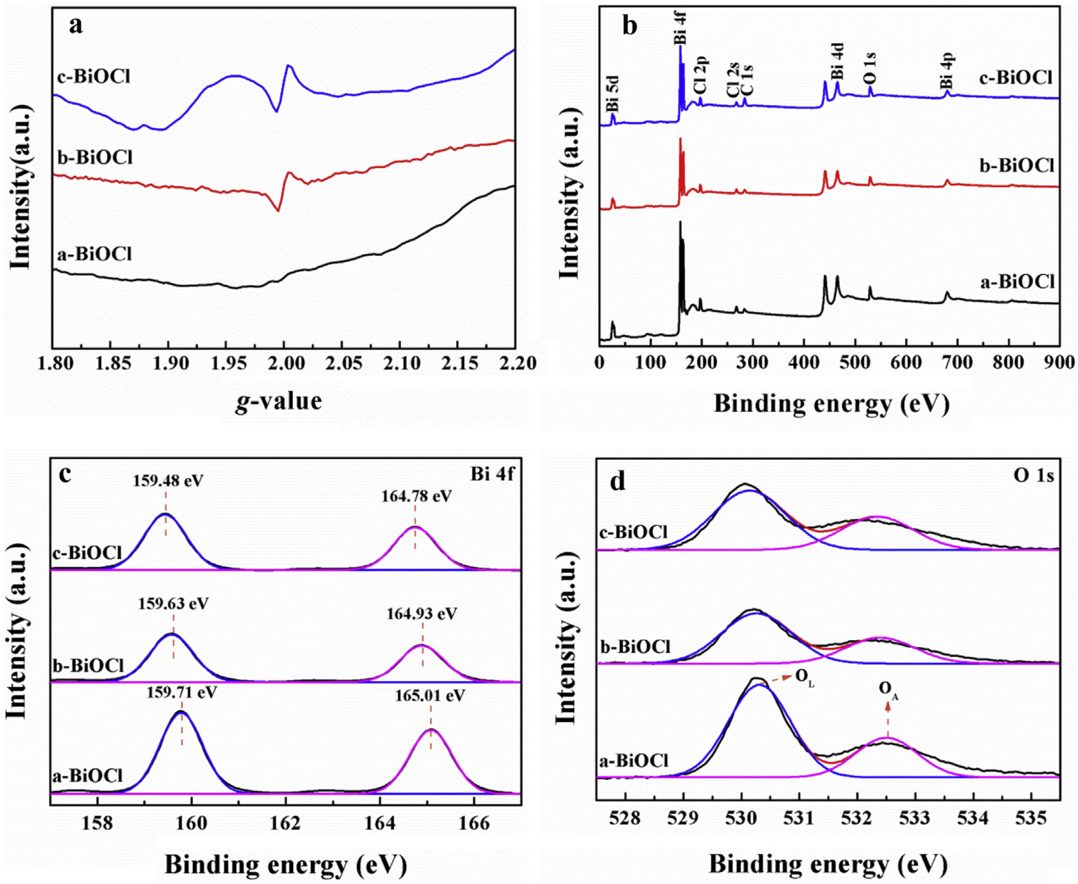

Fig. 4 – (a) Electron paramagnetic resonance (EPR) spectra, (b) X-ray photoelectron spectroscopy (XPS) survey spectra, (c) high-resolution Bi 4f spectra and (d) high-resolution O 1s spectra of a-BiOCl, b-BiOCl and c-BiOCl. O_L: crystal lattice oxygen; O_A: adsorbed oxygen species; *g*-value: dimensionless magnetic moment.

by the conventional solvothermal method. In contrast, there are no oxygen vacancies formed in the a-BiOCl sample synthesized by the precipitation method.

X-ray photoelectron spectroscopy (XPS, Escalab 250Xi, Thermo Fisher, USA) was further carried out to investigate the surface chemical structures of the three samples. The typical peaks corresponding to Bi 4f, O1s and Cl 2p are observed in the survey scan spectra (Fig. 4b), confirming the presence of these elements in all three samples. The high-resolution Bi 4f spectra are shown in Fig. 4c. The Bi $4f_{7/4}$ and Bi $4f_{5/4}$ peaks of a-BiOCl located at the binding energies of 159.7 and 165.0 eV with peak splitting of 5.3 eV can be readily assigned to Bi^{3+} in pure BiOCl (Wang et al., 2008a). Compared with a-BiOCl, the Bi 4f peaks of b-BiOCl and c-BiOCl were shifted to lower binding energy, which can be indexed to Bi in a lower valence state, resulting from the existence of oxygen vacancies (Mao et al., 2018; Ye et al., 2011). A similar phenomenon was also found in the TiO_2 system (Liu et al., 2009), in which the occurrence of oxygen vacancies led to a lower binding energy peak due to Ti^{3+}. Furthermore, the high-resolution O 1s spectra can be deconvoluted into two peaks (Fig. 4d). The binding energy at 530.1 eV can be assigned to crystal lattice oxygen (denoted as O_L), and the binding energy located at 532.2 eV corresponds to adsorbed oxygen species (denoted as O_A). It was reported that the chemisorbed oxygen component increases with the increase in oxygen vacancies (Huang et al., 2016; Zhang et al., 2015). Therefore, the concentrations of oxygen vacancies in photocatalysts can be roughly estimated by calculating the area ratio of O_A to O_L ($A(O_A/O_L)$). The calculated values of $A(O_A/O_L)$ were 0.36, 0.40 and 0.50 for a-BiOCl, b-BiOCl and c-BiOCl, respectively, which indicates that the oxygen vacancy concentrations follow the order of a-BiOCl < b-BiOCl < c-BiOCl. These results further confirm that the microwave solvothermal method could induce more surface oxygen vacancies on the materials, probably due to the intense localized heating effect resulting in ultrafast crystallization with surface defects.

2.2. Defluorination of PFOA and mechanisms

The decomposition of PFOA (50 μmol/L) by the three samples with simulated sunlight irradiation was investigated at natural pH 3.9 (Fig. 5a). It was found that direct photolysis by sunlight towards PFOA was very limited, suggesting that PFOA cannot be degraded by sunlight alone. In addition, no degradation was found in the dark control, indicating the BiOCl cannot degrade PFOA without light irradiation. Notably, when c-BiOCl was applied as the photocatalyst with sunlight

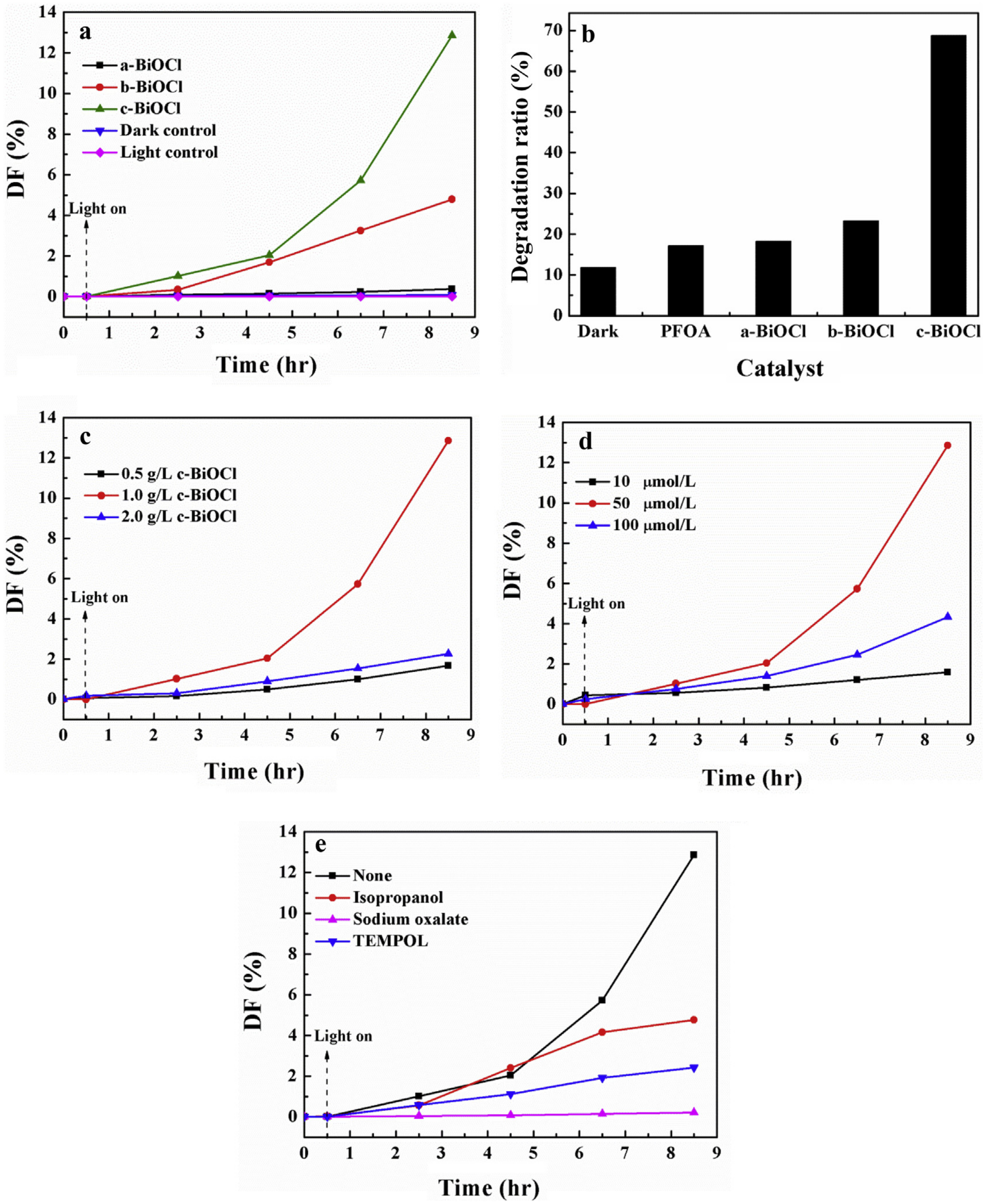

Fig. 5 – (a) Photocatalytic defluorination efficiency (DF) of perfluorooctanoic acid (PFOA) by the as-prepared samples under simulated sunlight irradiation. (b) Corresponding photocatalytic degradation efficiency of PFOA in 6.5 hr. Effects of (c) photocatalyst concentration, (d) PFOA concentration and (e) different scavengers on the defluorination efficiency of PFOA by c-BiOCl. TEMPOL: 4-hydroxy-2,2,6,6-tetramethylpiperidin-1-oxyl.

irradiation, the degradation of PFOA occurred, while F^- ions were steadily released into the solution with increasing reaction time. After 8.5 hr of sunlight irradiation, the defluorination efficiency could reach 12.86%, which was respectively 2.7 and 33.8 times larger than that using b-BiOCl (4.79%) and a-BiOCl (0.38%) as the photocatalysts. The degradation ratios of PFOA are demonstrated in Fig. 5b. It was found that the c-BiOCl exhibited a degradation efficiency of 68.8%, which was much higher than that of b-BiOCl (23.2%) and a-BiOCl without oxygen vacancies (18.3%). These results demonstrate that a photocatalyst surface with oxygen vacancies is much more beneficial for complete defluorination and mineralization rather than simply breaking the PFOA into short C–F chains.

The effects of photocatalyst concentration and PFOA concentration were also investigated to provide optimal parameters for practical use. As shown in Fig. 5c, with the concentration of catalyst increasing from 0.5 to 1.0 g/L, the defluorination ratio increases from 1.67% to 12.86%. Further increasing the catalyst concentration to 2.0 g/L, the defluorination ratio drops to 2.27%, which is due to the limited light penetration, catalyst aggregation and higher F^- adsorption when a high concentration of catalyst is used. In addition, a similar phenomenon was found for the effect of PFOA concentration. The defluorination efficiency first increased and then dropped with the increase of PFOA concentration from 10 to 100 μmol/L (Fig. 5d). Therefore, the optimal condition in the photocatalytic defluorination of PFOA by surface-defective BiOCl was identified as a catalyst concentration of 1.0 g/L with PFOA concentration of 50 μmol/L.

To understand the photocatalytic defluorination mechanism and the roles of reactive species, a scavenging study was conducted by adding specific chemical scavengers to trap potential reactive species. Isopropanol, TEMPOL and oxalate were used as •OH, $•O_2^-$ and photo-generated h^+ scavengers, respectively, according to previous studies (Wang et al., 2011, 2018). As shown in Fig. 5e, with isopropanol addition, the defluorination efficiency did not change very much in the first 6 hr, and was found to decrease slightly when the time was extended to 8.5 hr, suggesting that •OH plays a minor role in the PFOA defluorination process. This result was also found in previous studies, that •OH is ineffective for the PFOA defluorination process (Wang et al., 2017; Zhao et al., 2015). The addition of TEMPOL had a more obvious inhibition impact on the defluorination efficiency, suggesting that $•O_2^-$ plays a more significant role than that of •OH. Interestingly, adding oxalate was found to almost completely inhibit the defluorination process, and the defluorination efficiency dropped to only 0.22%. These results clearly demonstrate that photo-generated h^+ plays the most important role, while •OH and $•O_2^-$ appear to assist the photocatalytic defluorination process.

To further study the structure–property relationship between the photocatalysts and the defluorination efficiency, valence XPS spectra were conducted to study the edges of the valence band for the BiOCl samples. It was found that c-BiOCl exhibits typical DOS characteristics of a valence band, and the valence band edge energy was observed to be about 2.54 eV (Appendix A Fig. S2). Compared with those of b-BiOCl and a-BiOCl, the valence band edge of c-BiOCl was upshifted by 0.16 and 0.24 eV, respectively. In addition, rapid and reproducible photocurrent responses were evidenced with several repeated on/off light illumination cycles (Fig. 6a). In contrast, much lower photocurrent density was obtained for b-BiOCl and a-BiOCl. The average photocurrent density for the c-BiOCl electrode reached 3.85 $\mu A/cm^2$, while the photocurrent for b-BiOCl and a-BiOCl was only 0.74 and 0.40 $\mu A/cm^2$ under the same testing conditions. Therefore, the photocurrent for c-BiOCl was 5.2 and 9.6 times higher than that of b-BiOCl and a-BiOCl electrodes. Fig. 6b shows the EIS Nyquist plots of the BiOCl sample electrodes. The arc radius can be used as an indicator to evaluate the charge transfer efficiency on the electrodes (Wang et al., 2016). The arc radius of the samples follows the order of c-BiOCl < b-BiOCl < a-BiOCl electrode, suggesting that the charge separation and migration rates for photo-generated e^-–h^+ pairs is the highest on c-BiOCl, which is in agreement with the results of the above photocurrent measurements. This result further confirms that the photo-induced interface charge separation during the PFOA defluorination process can be promoted by the induced surface oxygen vacancies.

The photocatalytic mechanism for the defluorination of PFOA by oxygen vacancy-rich BiOCl is proposed. As shown in Fig. 7, when the BiOCl is excited by sunlight, photo-induced h^+ is produced in the valence band. The h^+ can direct react with surface-adsorbed PFOA to generate perfluorocarboxylate radicals, which are unstable and will undergo Photo-Kolbe reactions to lose terminal carboxylate groups to produce perfluoroalkane radicals (C_7F_{15}•) (Panchangam et al., 2009b) (Eqs. (3)–(4)). Meanwhile, the h^+ can also react with surface H_2O/OH^- to generate •OH, which will subsequently react with C_7F_{15}• to produce $C_7F_{15}OH$ (Eq. (5)). After a series of chemical reactions of HF elimination and hydrolysis, the PFOA would lose a CF_2 unit to produce $C_6F_{13}COOH$ (Eqs. (6)–(7)). Finally, complete defluorination and mineralization of PFOA are gradually achieved through similar pathways (Panchangam et al., 2009b):

$$C_7F_{15}COO^- + h^+ \rightarrow C_7F_{15}COO• \quad (3)$$

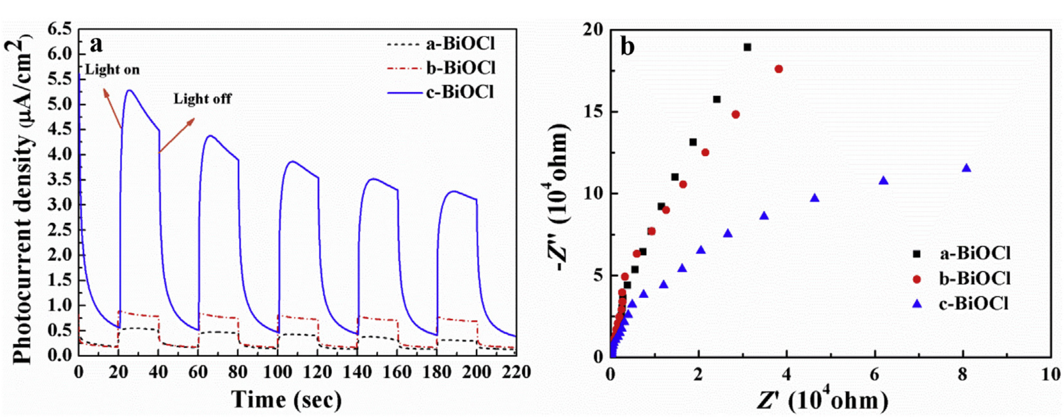

Fig. 6 – (a) Transient photocurrent responses under simulated sunlight irradiation and (b) electrochemical impedance spectroscopy (EIS) Nyquist plots for a-BiOCl, b-BiOCl and c-BiOCl. Z': real impedance; Z": imaginary impedance.

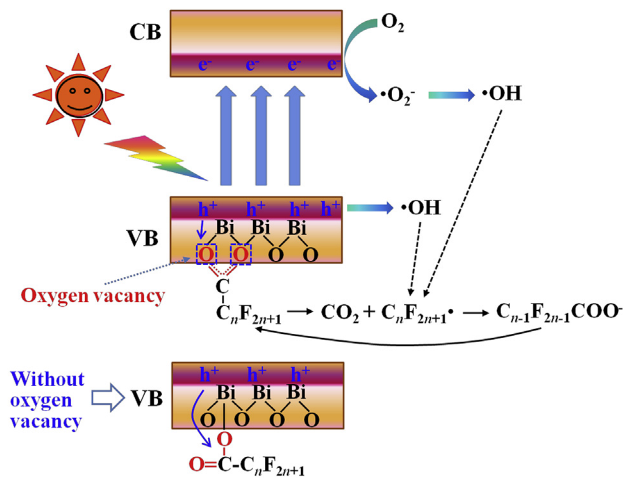

Fig. 7 – Schematic illustration of the mechanism of photocatalytic defluorination of PFOA by BiOCl with oxygen vacancies. CB: conduction band; VB: valance band; h^+: photo-generated hole; e^-: photo-generated electron.

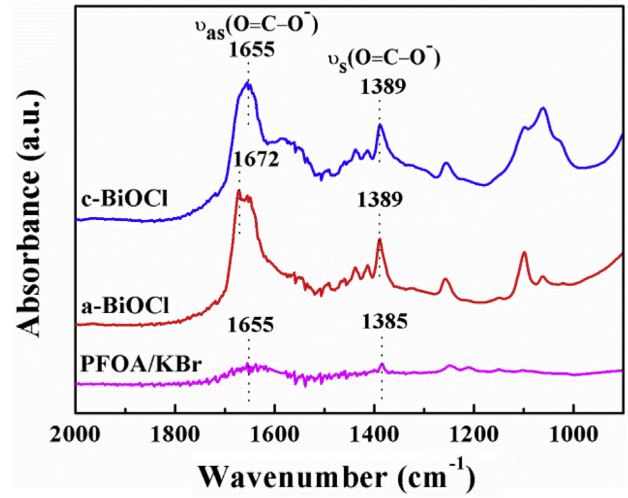

Fig. 8 – Diffuse reflectance infrared Fourier transform (DRIFT) spectra of PFOA adsorbed on a-BiOCl and c-BiOCl photocatalysts illustrating the different surface coordination states. $\nu_{as}(O{=}C{-}O^-)$: asymmetric stretches of carboxylate group; $\nu_s(O{=}C{-}O^-)$: symmetric stretches of carboxylate group.

$$C_7F_{15}COO\bullet \rightarrow C_7F_{15}\bullet + CO_2 \quad (4)$$

$$C_7F_{15}\bullet + \bullet OH \rightarrow C_7F_{15}OH \quad (5)$$

$$C_7F_{15}OH \rightarrow C_6F_{13}COF + HF \quad (6)$$

$$C_6F_{13}COF + H_2O \rightarrow C_6F_{13}COO^- + HF + H^+ \quad (7)$$

It should be noted that in this direct h^+-triggered defluorination process, the intimate contact between the photocatalyst surface and PFOA plays the most important role. According to previous studies (da Silva et al., 2017; Li et al., 2012, 2013a, 2013b), the terminal carboxylate group of PFOA can be readily coordinated to surface metal ions on metal oxides in monodentate or bidentate/bridging modes. To study the coordination modes of PFOA on the photocatalyst surface, DRIFTS (diffuse reflectance infrared Fourier transform spectroscopy (Nicolet IS10, Thermo Fisher, USA) measurements were conducted, which is a supersensitive method to detect fine structural changes of adsorbed species. Fig. 8 shows the DRIFTS spectrum of adsorbed PFOA on BiOCl with and without oxygen vacancies. For PFOA/KBr, IR absorption peaks at 1457 and 1660 cm^{-1} were observed, corresponding to the symmetric ($\nu_s(COO^-)$) and asymmetric stretches ($\nu_{as}(COO^-)$) of the carboxylate group, respectively. These peak positions are changed for PFOA/BiOCl, confirming that PFOA coordinates with BiOCl via its carboxylate group. In addition, the coordination configuration can be identified by studying the difference in stretching frequencies of the carboxylate group ($\Delta\nu = \nu_{as}(COO^-) - \nu_s(COO^-)$) (Li et al., 2012). It has been reported that a monodentate coordination is dominant if the $\Delta\nu$ value is larger than the ionic $\Delta\nu$, while a bidentate/bridging coordination occurs if the $\Delta\nu$ value is smaller than the ionic $\Delta\nu$. In this study, the $\Delta\nu$ value observed for PFOA/a-BiOCl (283 cm^{-1}) is clearly larger than that of the PFOA salt (270 cm^{-1}), suggesting that PFOA coordinates to a-BiOCl (without oxygen vacancies) in a monodentate mode. In contrast, the $\Delta\nu$ value for PFOA/c-BiOCl (266 cm^{-1}) is lower than ionic $\Delta\nu$, which indicates that PFOA is bound to c-BiOCl (with oxygen vacancy) in a bidentate/bridging mode. Therefore, the carboxyl group of PFOA is expect to be anchored on the oxygen vacancy to coordinate with Bi^{3+} in a bidentate/bridging mode (Fig. 7); thus, covalent bonding between PFOA and c-BiOCl is observed, which will significantly facilitate direct h^+ attack. In addition, it has been recognized that oxygen vacancies can also form defective states, which are located close to the conduction band bottom. The defective states are expected to capture photo-induced e^- and further inhibit charge recombination, prolonging the lifetime of photo-induced h^+. Therefore, c-BiOCl, with the highest concentration of oxygen vacancies, exhibits the highest defluorination efficiency for PFOA.

3. Conclusions

In summary, to solve the environmental problem caused by perfluorocarboxylic compounds, BiOCl with oxygen vacancies was fabricated by a microwave solvothermal method and utilized as photocatalyst to decompose PFOA under sunlight irradiation. Compared with conventional solvothermal and precipitation methods, the microwave solvothermal method could introduce more surface oxygen vacancies on BiOCl due to localized heating effects; this might serve as a general method to synthesize surface-defective materials. The as-prepared BiOCl showed greatly enhanced photocatalytic defluorination efficiency, which was 2.7 and 33.8 times higher than that of BiOCl fabricated by the conventional solvothermal and precipitation methods, respectively. The surface oxygen vacancies played the crucial role of coordinating with the carboxylate group of PFOA as well as inhibiting the undesired e^-–h^+ recombination by forming defect states within the band structure; thus, more photo-generated h^+ could be used for defluorination via the direct h^+ attack pathway. As a proof-of-concept, this work provides useful information to establish a universal strategy to photocatalytically treat perfluorocarboxylic compounds by taking advantage of surface oxygen vacancies, which can be easily realized by broadly applicable and fast microwave-assisted methods.

Acknowledgments

This work was supported by the National Natural Science Foundation of China (Nos. 21607028, 41425015 and 41573086), the Research Grant Council of Hong Kong Special Administrative Region (SAR) Government (No. GRF14100115), Science and Technology Project of Guangdong Province, China (No. 2017A050506049), Local Innovative and Research Teams Project of Guangdong Pearl River Talents Program (No. 2017BT01Z032), Innovation Team Project of Guangdong Provincial Department of Education (No. 2017KCXTD012) and Leading Scientific, Technical and Innovation Talents of Guangdong Special Support Program (No. 2016TX03Z094).

Appendix A. Supplementary data

Supplementary data to this article can be found online at https://doi.org/10.1016/j.jes.2019.04.012.

REFERENCES

Chen, X., Wang, W.J., Chen, X.Y., Bi, J.H., Wu, L., Li, Z.H., et al., 2009. Microwave hydrothermal synthesis and upconversion properties of $NaYF_4$:Yb^{3+}, Tm^{3+} with microtube morphology. Mater. Lett. 63, 1023–1026.

Cui, D.D., Wang, L., Xu, K., Ren, L., Wang, L., Yu, Y.X., et al., 2018. Band-gap engineering of BiOCl with oxygen vacancies for efficient photooxidation properties under visible-light irradiation. J. Mater. Chem. A 6, 2193–2199.

Cushing, S.K., Meng, F.K., Zhang, J.Y., Ding, B.F., Chen, C.K., Chen, C.J., et al., 2017. Effects of defects on photocatalytic activity of hydrogen-treated titanium oxide nanobelts. ACS Catal. 7, 1742–1748.

da Silva, F.L., Laitinen, T., Pirila, M., Keiski, R.L., Ojala, S., 2017. Photocatalytic degradation of perfluorooctanoic acid (PFOA) from wastewaters by TiO_2, In_2O_3 and Ga_2O_3 catalysts. Top. Catal. 60, 1345–1358.

Dong, F., Xiao, X., Jiang, G.M., Zhang, Y.X., Cui, W., Ma, J.Z., 2015. Surface oxygen-vacancy induced photocatalytic activity of La$(OH)_3$ nanorods prepared by a fast and scalable method. Phys. Chem. Chem. Phys. 17, 16058–16066.

Hassan, N.S., Jalil, A.A., Triwahyono, S., Khusnun, N.F., Izan, S.M., Kidam, K., et al., 2018. Synergistic effect of microwave rapid heating and weak mineralizer on silica-stabilized tetragonal zirconia nanoparticles for enhanced photoactivity of Bisphenol A. J. Mol. Liq. 261, 423–430.

Hu, J.L., Fan, W.J., Ye, W.Q., Huang, C.J., Qiu, X.Q., 2014. Insights into the photosensitivity activity of BiOCl under visible light irradiation. Appl. Catal. B Environ. 158, 182–189.

Huang, Y., Li, H., Fan, W., Zhao, F., Qiu, W., Ji, H., et al., 2016. Defect engineering of bismuth oxyiodide by IO_3^- doping for increasing charge transport in photocatalysis. ACS Appl. Mater. Interfaces 8, 27859–27867.

Kashinath, L., Namratha, K., Byrappa, K., 2015. Microwave assisted facile hydrothermal synthesis and characterization of zinc oxide flower grown on graphene oxide sheets for enhanced photodegradation of dyes. Appl. Surf. Sci. 357, 1849–1856.

Kim, Y., Kim, H.B., Jang, D.J., 2014. Facile microwave fabrication of CdS nanobubbles with highly efficient photocatalytic performances. J. Mater. Chem. A 2, 5791–5799.

Kong, M., Li, Y.Z., Chen, X., Tian, T.T., Fang, P.F., Zheng, F., et al., 2011. Tuning the relative concentration ratio of bulk defects to surface defects in TiO_2 nanocrystals leads to high photocatalytic efficiency. J. Am. Chem. Soc. 133, 16414–16417.

Lee, Y.C., Lo, S.L., Kuo, J., Huang, C.P., 2013. Promoted degradation of perfluorooctanic acid by persulfate when adding activated carbon. J. Hazard. Mater. 261, 463–469.

Li, X.Y., Zhang, P.Y., Jin, L., Shao, T., Li, Z.M., Cao, J.J., 2012. Efficient photocatalytic decomposition of perfluorooctanoic acid by indium oxide and its mechanism. Environ. Sci. Technol. 46, 5528–5534.

Li, Z.M., Zhang, P.Y., Li, J.G., Shao, T., Jin, L., 2013a. Synthesis of In_2O_3-graphene composites and their photocatalytic performance towards perfluorooctanoic acid decomposition. J. Photochem. Photobiol. A Chem. 271, 111–116.

Li, Z.M., Zhang, P.Y., Shao, T., Wang, J.L., Jin, L., Li, X.Y., 2013b. Different nanostructured In_2O_3 for photocatalytic decomposition of perfluorooctanoic acid (PFOA). J. Hazard. Mater. 260, 40–46.

Li, H., Shi, J.G., Zhao, K., Zhang, L.Z., 2014. Sustainable molecular oxygen activation with oxygen vacancies on the {001} facets of BiOCl nanosheets under solar light. Nanoscale 6, 14168–14173.

Lin, H., Niu, J.F., Liang, S.T., Wang, C., Wang, Y.J., Jin, F.Y., et al., 2018. Development of macroporous Magneli phase Ti_4O_7 ceramic materials: as an efficient anode for mineralization of poly- and perfluoroalkyl substances. Chem. Eng. J. 354, 1058–1067.

Lindstrom, A.B., Strynar, M.J., Libelo, E.L., 2011. Polyfluorinated compounds: past, present, and future. Environ. Sci. Technol. 45, 7954–7961.

Liu, G., Yang, H.G., Wang, X.W., Cheng, L.N., Lu, H.F., Wang, L.Z., et al., 2009. Enhanced photoactivity of oxygen-deficient anatase TiO_2 sheets with dominant {001} facets. J. Phys. Chem. C 113, 21784–21788.

Liu, Y.F., Ma, L., Yang, Q., Li, G.H., Zhang, F., 2018. Occurrence and spatial distribution of perfluorinated compounds in groundwater receiving reclaimed water through river bank infiltration. Chemosphere 211, 1203–1211.

Mao, C.L., Cheng, H.G., Tian, H., Li, H., Xiao, W.J., Xu, H., et al., 2018. Visible light driven selective oxidation of amines to imines with BiOCl: does oxygen vacancy concentration matter? Appl. Catal. B Environ. 228, 87–96.

Moriwaki, H., Takagi, Y., Tanaka, M., Tsuruho, K., Okitsu, K., Maeda, Y., 2005. Sonochemical decomposition of perfluorooctane sulfonate and perfluorooctanoic acid. Environ. Sci. Technol. 39, 3388–3392.

Pan, X.Y., Yang, M.Q., Fu, X.Z., Zhang, N., Xu, Y.J., 2013. Defective TiO_2 with oxygen vacancies: synthesis, properties and photocatalytic applications. Nanoscale 5, 3601–3614.

Panchangam, S.C., Lin, A.Y.C., Tsai, J.H., Lin, C.F., 2009a. Sonication-assisted photocatalytic decomposition of perfluorooctanoic acid. Chemosphere 75, 654–660.

Panchangam, S.C., Lin, A.Y.C., Shaik, K.L., Lin, C.F., 2009b. Decomposition of perfluorocarboxylic acids (PFCAs) by heterogeneous photocatalysis in acidic aqueous medium. Chemosphere 77, 242–248.

Sahu, S.P., Qanbarzadeh, M., Ateia, M., Torkzadeh, H., Maroli, A.S., Cates, E.L., 2018. Rapid degradation and mineralization of perfluorooctanoic acid by a new petitjeanite $Bi_3O(OH)(PO_4)_2$ microparticle ultraviolet photocatalyst. Environ. Sci. Technol. Lett. 5, 533–538.

Shao, T., Zhang, P.Y., Jin, L., Li, Z.M., 2013. Photocatalytic decomposition of perfluorooctanoic acid in pure water and sewage water by nanostructured gallium oxide. Appl. Catal. B Environ. 142, 654–661.

Sinclair, E., Kannan, K., 2006. Mass loading and fate of perfluoroalkyl surfactants in wastewater treatment plants. Environ. Sci. Technol. 40, 1408–1414.

Skutlarek, D., Exner, M., Farber, H., 2006. Perfluorinated surfactants in surface and drinking water. Environ. Sci. Pollut. Res. 13, 299–307.

Song, Z., Dong, X.L., Wang, N., Zhu, L.H., Luo, Z.H., Fang, J.D., et al., 2017. Efficient photocatalytic defluorination of perfluorooctanoic acid over BiOCI nanosheets via a hole direct oxidation mechanism. Chem. Eng. J. 317, 925–934.

Song, P.Y., Li, D.Y., Wang, X.D., Zhong, X.H., 2018. Effects of perfluorooctanoic acid exposure during pregnancy on the reproduction and development of male offspring mice. Andrologia 50 (8).

Stanifer, J.W., Stapleton, H.M., Souma, T., Wittmer, A., Zhao, X.L., Boulware, L.E., 2018. Perfluorinated chemicals as emerging environmental threats to kidney health: a scoping review. Clin. J. Am. Soc. Nephrol. 13, 1479–1492.

Sun, T.W., Zhu, Y.J., Qi, C., Ding, G.J., Chen, F., Wu, J., 2016. α-Fe_2O_3 nanosheet-assembled hierarchical hollow mesoporous microspheres: microwave-assisted solvothermal synthesis and application in photocatalysis. J. Colloid Interface Sci. 463, 107–117.

Sungur, S., 2018. Dietary exposure to perfluorooctanoic acid (PFOA) and perfluorooctane sulfonic acid (PFOS): a review of recent literature. Toxin Rev. 37, 106–116.

Tang, H.Q., Xiang, Q.Q., Lei, M., Yan, J.C., Zhu, L.H., Zou, J., 2012. Efficient degradation of perfluorooctanoic acid by UV-Fenton process. Chem. Eng. J. 184, 156–162.

Tian, J., Shao, Q., Zhao, J., Pan, D., Dong, M., Jia, C., et al., 2019. Microwave solvothermal carboxymethyl chitosan templated synthesis of TiO_2/ZrO_2 composites toward enhanced photocatalytic degradation of Rhodamine B. J. Colloid Interface Sci. 541, 18–29.

Wang, C.H., Shao, C.L., Liu, Y.C., Zhang, L., 2008a. Photocatalytic properties BiOCl and Bi_2O_3 nanofibers prepared by electrospinning. Scripta Mater. 59, 332–335.

Wang, W.J., Bi, J.H., Wu, L., Li, Z.H., Wang, X.X., Fu, X.Z., 2008b. Hydrothermal synthesis and performance of a novel nanocrystalline $Pb_2Sn_2O_6$ photocatalyst. Nanotechnology 19, 505705.

Wang, W.J., Zhang, L.Z., An, T.C., Li, G.Y., Yip, H.Y., Wong, P.K., 2011. Comparative study of visible-light-driven photocatalytic mechanisms of dye decolorization and bacterial disinfection by B-Ni-codoped TiO_2 microspheres: the role of different reactive species. Appl. Catal. B Environ. 108, 108–116.

Wang, W.J., Ng, T.W., Ho, W.K., Huang, J.H., Liang, S.J., An, T.C., et al., 2013. $CdIn_2S_4$ microsphere as an efficient visible-light-driven photocatalyst for bacterial inactivation: synthesis, characterizations and photocatalytic inactivation mechanisms. Appl. Catal. B Environ. 129, 482–490.

Wang, W.J., Li, Y.C., Kang, Z.W., Wang, F., Yu, J.C., 2016. A NIR-driven photocatalyst based on α-$NaYF_4$:Yb, Tm@TiO_2 core-shell structure supported on reduced graphene oxide. Appl. Catal. B Environ. 182, 184–192.

Wang, S.N., Yang, Q., Chen, F., Sun, J., Luo, K., Yao, F.B., et al., 2017. Photocatalytic degradation of perfluorooctanoic acid and perfluorooctane sulfonate in water: a critical review. Chem. Eng. J. 328, 927–942.

Wang, W.J., Li, G.Y., An, T.C., Chan, D.K.L., Yu, J.C., Wong, P.K., 2018. Photocatalytic hydrogen evolution and bacterial inactivation utilizing sonochemical-synthesized g-C_3N_4/red phosphorus hybrid nanosheets as a wide-spectral-responsive photocatalyst: the role of type I band alignment. Appl. Catal. B Environ. 238, 126–135.

Xu, J.J., Wu, M.M., Yang, J.W., Wang, Z.M., Chen, M.D., Teng, F., 2017. Efficient photocatalytic degradation of perfluorooctanoic acid by a wide band gap p-block metal oxyhydroxide InOOH. Appl. Surf. Sci. 416, 587–592.

Ye, L.Q., Zan, L., Tian, L.H., Peng, T.Y., Zhang, J.J., 2011. The {001} facets-dependent high photoactivity of BiOCl nanosheets. Chem. Commun. 47, 6951–6953.

Zhang, L., Wang, W.Z., Jiang, D., Gao, E.P., Sun, S.M., 2015. Photoreduction of CO_2 on BiOCl nanoplates with the assistance of photoinduced oxygen vacancies. Nano Res. 8, 821–831.

Zhang, X.F., Wang, Y.N., Liu, B.S., Sang, Y.H., Liu, H., 2017. Heterostructures construction on TiO_2 nanobelts: a powerful tool for building high-performance photocatalysts. Appl. Catal. B Environ. 202, 620–641.

Zhao, B.X., Lv, M., Zhou, L., 2012. Photocatalytic degradation of perfluorooctanoic acid with β-Ga_2O_3 in anoxic aqueous solution. J. Environ. Sci. 24, 774–780.

Zhao, K., Zhang, L.Z., Wang, J.J., Li, Q.X., He, W.W., Yin, J.J., 2013. Surface structure-dependent molecular oxygen activation of BiOCl single-crystalline nanosheets. J. Am. Chem. Soc. 135, 15750–15753.

Zhao, B.X., Li, X., Yang, L., Wang, F., Li, J.C., Xia, W.X., et al., 2015. β-Ga_2O_3 nanorod synthesis with a one-step microwave irradiation hydrothermal method and its efficient photocatalytic degradation for perfluorooctanoic acid. Photochem. Photobiol. 91, 42–47.

Zhong, J.B., Zhao, Y.K., Ding, L.Y., Ji, H.W., Ma, W.H., Chen, C.C., et al., 2019. Opposite photocatalytic oxidation behaviors of BiOCl and TiO_2: direct hole transfer vs. indirect •OH oxidation. Appl. Catal. B Environ. 241, 514–520.